Astronomical Techniques and Instruments, Vol. 2, November 2025, 388–399

Article Open Access

Evaluating the regional consistency of astronomical observing conditions across Dome A

Kaiwen Zheng[1,2,3], Kun Ma[1,2,4], Jiali Chen[1,2,3], Haosi Song[5], Tiancong Zhang[5], Shiyi Wang[5], Han Wang[5], Peng Jiang[6*], Xiaoyan Li[1,2*]

[1]*Nanjing Institute of Astronomical Optics & Technology*, *Chinese Academy of Sciences*, *Nanjing* 210042, *China*

[2]*CAS Key Laboratory of Astronomical Optics & Technology*, *Nanjing Institute of Astronomical Optics & Technology*, *Nanjing* 210042, *China*

[3]*University of Chinese Academy of Sciences*, *Beijing* 100049,*China*

[4]*School of Optoelectronic Engineering*, *Changchun University of Science and Technology*, *Changchun* 130022, *China*

[5]*Bell Honors School*, *Nanjing University of Posts and Telecommunications*, *Nanjing* 210023, *China*

[6]*Polar Research Institute of China*, *Shanghai* 200136, *China*

*Correspondences: jiangpeng@pric.org.cn; xyli@niaot.ac.cn

Received: July 7, 2025; Accepted: September 2, 2025; Published Online: September 3, 2025; https://doi.org/10.3724/ati2025061; https://cstr.cn/32083.14.ati2025061

© 2025 Editorial Office of Astronomical Techniques and Instruments, Yunnan Observatories, Chinese Academy of Sciences. This is an open access article under the CC BY 4.0 license (http://creativecommons.org/licenses/by/4.0/)

Citation: Zheng, K. W., Ma, K., Chen, J. L., et al. 2025. Evaluating the regional consistency of astronomical observing conditions across Dome A. *Astronomical Techniques and Instruments*, **2**(6): 388−399. https://doi.org/10.3724/ati2025061.

Abstract: With excellent seeing conditions, ultra-low infrared background noise, high frequency of space debris transits, and continuous polar night coverage, Dome A in Antarctica has become an ideal platform for ground-based astronomy and space situational monitoring. As a crucial observatory site for international deep space, deep Earth, deep sea, and polar exploration, it is very important to evaluate the suitability of Dome A as an observatory site. However, owing to extreme environmental constraints, the evaluation of site conditions is mainly based on single-point measurements, making it challenging to comprehensively evaluate the effective site range and uniformity. This study integrated satellite remote sensing data to develop a cross-comparison framework for diverse indicators across Dome A, to evaluate its spatial uniformity. We find that the area surrounding the Dome A site, defined within a roughly 1° × 1° latitude and longitude range, possesses excellent astronomical observation conditions.

Keywords: Dome A; Cloud cover; Vertical wind shear; Skin temperature; Net solar radiation; Climate stability

1. INTRODUCTION

The highest point of the Antarctic, Dome A, was explored during the Chinese 21st Antarctic Scientific Expedition in 2004–2005. Subsequent studies have shown that Dome A provides ideal conditions for terrestrial optical, infrared, and submillimeter astronomical observations[1]. Measurements acquired using the Kunlun Differential Image Motion Monitor (KL-DIMM) at Kunlun Station, in Antarctica, show that a telescope mounted on an 8-meter-high tower has a 31% probability of avoiding near-ground turbulence, with a median seeing of 0.31"[2]. The low temperatures (−80°C to −60°C) and dry conditions (water vapor column density < 0.1 mm) at Kunlun Station result in extremely low near-infrared background radiation. We measured the sky background intensity at Kunlun Station, using the Near-Infrared Sky Brightness Monitor (NISBM) instrument, for the J, H, and Ks bands as 600–1 100 μJy arcsec^{-2}, 1 100–2 600 μJy arcsec^{-2}, and 200–900 μJy arcsec^{-2}, respectively[3]. In addition, owing to the orbits of space debris converging over the South Pole, the frequency of space debris that transits over Dome A is significantly higher than at other mid-latitude sites, providing Dome A with a unique advantage for long-term space debris monitoring. In near-Earth orbit, 82.6% of all space debris passes over Kunlun Station during every orbital revolution, while 93.7% of debris passes over Kunlun Station during more than half of its orbital revolutions. As the only ground-based site on Earth capable of providing long-term observation near the South Celestial Pole, Antarctica fills the observation gap left by Northern Hemisphere sites such as Hawaii and Qinghai, serving as a crucial strategic node in the global astronomical observation network. In addition, the prolonged polar night, lasting several months during the Antarctic winter, allows telescopes to conduct uninterrupted observations for up to

2670 h, significantly enhancing the observational efficiency of time-domain astronomy (for targets such as supernova explosions and afterglow tracking of gravitational wave events)[4].

Owing to technical constraints imposed by extreme environmental conditions, the current site performance evaluation for Dome A relies mainly on single-point measurements. Several key instruments have been deployed at Kunlun Station, including the Chinese Small Telescope Array (CSTAR)[5], Antarctic Schmidt Telescopes (AST3)[6], and the Antarctic 15 cm NIR Telescope[7], which have already validated the scientific potential of extreme Antarctic astronomical sites. A planned J/H/K-band near-infrared telescope, with an aperture of 0.5–1 m, will further enhance this astronomical site as a core station for multiband observations. Building on existing single-point site data from Dome A, a further systematic assessment of the observation conditions in the surrounding areas of the single-point can quantitatively analyze the site capacity at Kunlun Station. This will provide a scientific basis for resource allocation for future large telescope construction, very long baseline interferometry (VLBI) arrays, and large-scale space debris monitoring networks at Dome A.

We selected a 1° × 1° geographic area in latitude and longitude, defined using the geographic coordinate system, surrounding Dome A as the research region. By using multi-source remote sensing data, meteorological data, and other resources, we obtained evaluation parameters such as cloud cover, total precipitation, total column water vapor, skin temperature, vertical wind shear (VWS), and net surface solar radiation within this defined area around Dome A. Using remote sensing and Geographic Information System (GIS) techniques, we analyzed the spatiotemporal distribution characteristics of these parameters over long time series and their relationship with optical astronomical observations.

2. OBSERVATIONS AND DATA

Using multi-source remote sensing data and high-precision meteorological data, we conducted an in-depth analysis of the suitability of Dome A and its surrounding areas for astronomical observations, in terms of cloud cover, total precipitation, total column water vapor, skin temperature, VWS, and net surface solar radiation. The cloud cover analysis in this study used the Cloud, Albedo and Surface Radiation dataset from Advanced Very High Resolution Radiometer (AVHRR) data-second edition (CLARA-A2), which is provided by the Climate Monitoring Satellite Application Facility (CM SAF) at the European Organization for the Exploitation of Meteorological Satellites (EUMETSAT). This dataset is based on observations from multiple satellites equipped with AVHRR sensors, which have been uniformly processed to generate long-term climate data products. The cloud cover data provided by CLARA-A2 has a spatial resolution of 0.25° × 0.25° and a temporal resolution of 1 h. It can be used to study the distribution of cloud cover on a large scale, together with its evolutionary trends. Here, we used the total cloud cover variable provided in the dataset, which represents the proportion of the observation area covered by cloud at any given time and location.

The fifth-generation reanalysis dataset from the European Centre for Medium Range Weather Forecasts (ECMWF), ERA5, was used in this study. The variables, including net surface solar radiation, skin temperature, total precipitation, total column water vapor, and U-component and V-component of wind data were obtained from different sub-products of ERA5. Among them, the net surface solar radiation and total column water vapor data were from ERA5 hourly data on single levels, which contain data from 1940 to the present. We selected daily net surface solar radiation data for January, April, July, and October 2017, with a time accuracy of 1 h, a spatial resolution of 0.25° × 0.25°, and a data set unit of W m^{-2}. We used total column water vapor data for the entire year of 2017, with a temporal resolution of 1 h, a spatial resolution of 0.25° × 0.25°, and a dataset unit of kg m^{-2}. Skin temperature and total precipitation data were obtained from the ERA5-Land monthly averaged dataset, which contains data from 1950 to the present. We selected skin temperature and total precipitation data for the whole year of 2017, with a time resolution of 1 h and a spatial resolution of 0.1° × 0.1°. Skin temperature is measured in K, and total precipitation is measured in mm. We derived the U-component and V-component of wind data from the ERA5 hourly data on pressure levels, which contains data from 1940 to the present, and selected the U-component and V-component of wind data at the 350 hPa and 600 hPa pressure levels for January, April, July, and October 2017, with a temporal resolution of 1 h, a spatial resolution of 0.25° × 0.25°, and units of m s^{-1}.

3. CLOUD COVER

In this study, we used the CLARA-A2 dataset obtained from the American National Oceanic and Atmospheric Administration (NOAA) polar-orbiting satellite AVHRR sensor[8], selecting cloud cover spatial distribution data for January, April, July, and October of 2017. The cloud cover data for the target region (76.96°E–77.96°E, 79.88°S–80.88°S) were processed and analyzed to investigate seasonal variations, spatial distribution characteristics, and assess their suitability for astronomical observations.

In this dataset, cloud cover is defined as the percentage of the atmospheric column in each grid cell that is covered by clouds, averaged over a time scale (such as monthly averages). In other words, it represents the average cloud cover in the entire atmospheric column from the ground to the top of the troposphere during the observation period, which is a spatiotemporal composite average rather than an instantaneous observation or single-layer measurement. As shown in Fig. 1, the mean cloud cover

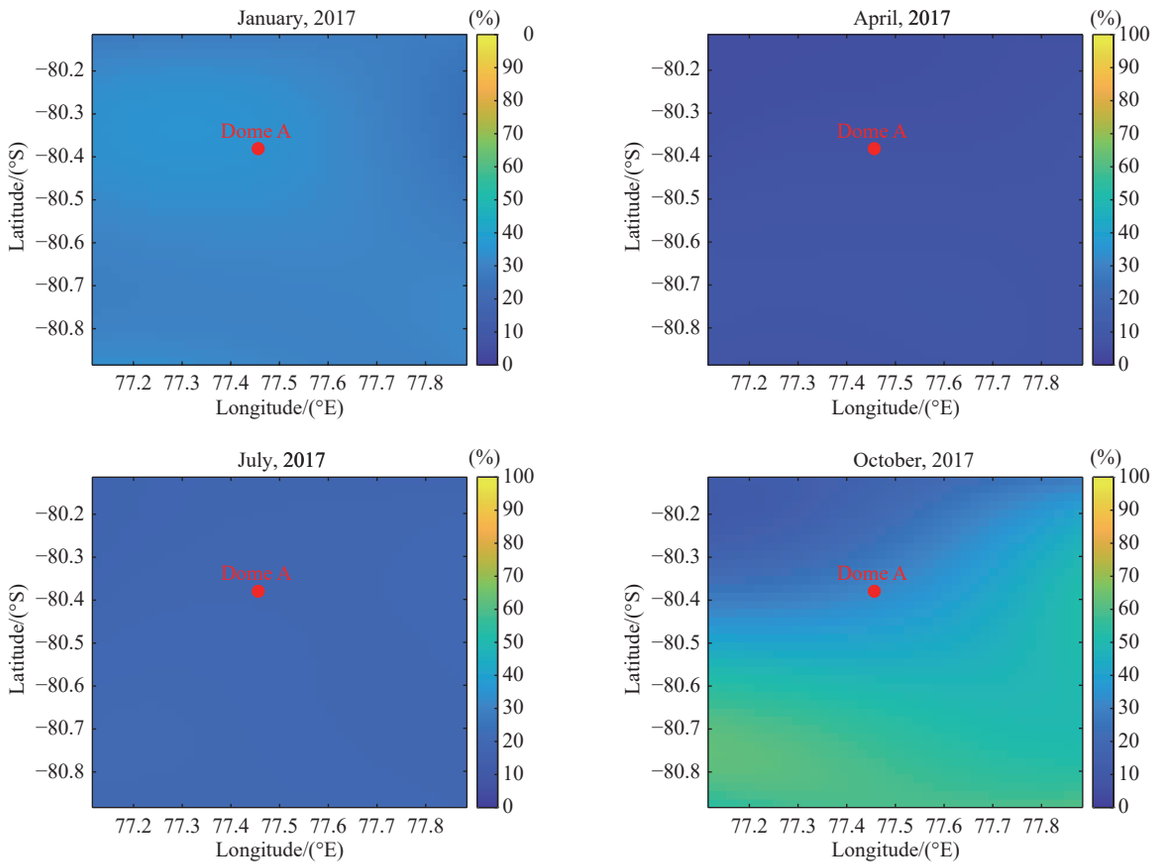

Fig. 1. Mean cloud fraction for Dome A and its surrounding areas in January, April, July, and October 2017.

range for Dome A and its surrounding areas in January, April, July, and October 2017 was 25%–35%, 5%–9%, 17%–20%, and 12%–60%, respectively. The monthly mean cloud cover for January, April, July, and October 2017 was 30.5%, 7.38%, 19%, and 41.31%. The cloud cover in this region is generally low, with distinct seasonal variation. The spatial resolution of the cloud cover dataset here is 0.25°. We performed precise data cropping for the target region, but the image was plotted based on grid points, rather than being reconstructed centered on Dome A, meaning that Dome A is not exactly at the center of the target area. In the visualization stage, we applied a two-dimensional interpolation smoothing process to the images generated from the raw data, to improve the spatial smoothness of the images without affecting the statistical analysis results of the original data.

Regarding spatial distribution, except for October, there is no significant monthly gradient variation in cloud cover within the 1° × 1° area surrounding Dome A. In October, the cloud cover exhibits a pattern with more in the south and less in the north. On the basis of the cloud cover variation trends in Fig. 2 for Dome A and its surrounding areas, the mean cloud cover from March to June is relatively low, indicating that this period may provide more favorable observation conditions, especially for observations requiring high atmospheric transparency (e.g., infrared telescopes). By contrast, the high variability in cloud cover during October should be considered when designing scientific equipment for interference resistance. This seasonal variation trend is strongly consistent with the findings of Saunders et al.[9], who reported that winter cloud cover at multiple Antarctic observation stations is generally low (approximately 20%), while summer cloud cover is relatively high (approximately 50%). This seasonal variation trend not only further validates the rationality of the findings in this study, but also confirms, from a global perspective, the characteristic of extremely high clear-sky rates at Dome A during the Antarctic winter. Furthermore, a comparative analysis with the Big Telescope Alt-azimuthal (BTA) site of the Special Astrophysical Observatory (SAO) of the Russian Academy of Sciences, which hosts the largest optical telescope in Eurasia, further highlights the advantages of Dome A. According to a study by Shikhovtsev et al.[10], based on reanalysis data from the National Centers for Environmental Prediction/National Center for Atmospheric Research (NCEP/NCAR), the annual mean total cloud cover in the BTA region in 2017 was 38.5%. By contrast, the total annual mean cloud cover over Dome A and its surrounding regions in our study was 20.57% in 2017, indicating significantly lower annual cloud cover and better clear-sky conditions.

Spatial variability can be comprehensively evaluated using coefficients of variation (CV), standard deviation (σ), and mean (μ), with the results presented in Table 1. April, at the beginning of polar night, shows an extremely low cloud cover in the region, indicating excellent observa-

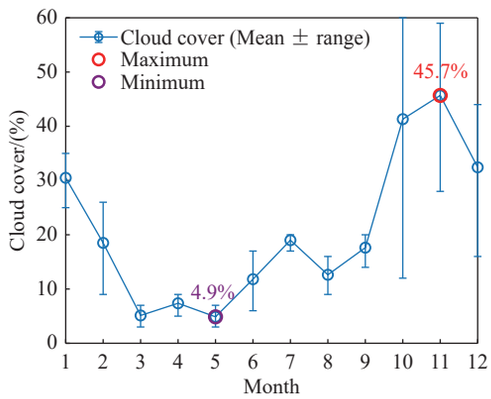

Fig. 2. Monthly mean cloud cover variation trend for Dome A and its surrounding areas in 2017.

tional potential. In July, the CV of cloud cover was only 0.05, and the standard deviation was also very low, reflecting the high uniformity in the cloud cover distribution of the target area. We found that the low cloud cover levels and their stability in April and July provide comparatively excellent meteorological conditions for astronomical observations.

Notably, the cloud cover measured by satellite remote sensing used in this study differs from that measured by ground-based panoramic cameras. In satellite remote sensing, cloud cover is mainly determined based on data from the visible light and infrared bands. This is obtained by analyzing parameters such as surface reflectance, brightness temperature, and cloud top characteristics, combined with cloud detection algorithms (such as thresholding and machine learning classification), to determine whether clouds cover a pixel. All-sky cameras capture 360° all-sky images from the ground upward. By combining human visual interpretation with algorithms that automatically identify image differences, this can distinguish between cloud-covered and clear-sky areas in the images. Because all-sky cameras are suitable for local high-precision, high-frequency cloud quantity monitoring, while remote sensing technology is more suitable for large-scale, multi-parameter cloud characteristic inversion, the two technologies are complementary in terms of astronomical site selection. Given that this study focuses on analyzing the large-scale site uniformity of Dome A, we used remote sensing data. According to Yang et al.[11], based on all-sky camera observations in the Dome A region, approximately 83.3% of the time between January 17, 2017, and May 28, 2018, was cloud-free, providing a good reflection of the frequency of cloud-free conditions over time. Satellite remote sensing, however, provides spatial cloud cover, which is the proportion of the area covered by clouds at a given time. Based on satellite remote sensing data, we calculated that the average cloud cover for the region in 2017 was 20.57%. Owing to fundamental differences in statistical methods and data definitions, the two cannot be directly compared quantitatively. Nevertheless, both data sources point to the fact that Dome A has an extremely high clear-sky rate during winter nights. This indirectly reflects the accuracy of satellite remote sensing data.

Table 1. Statistical characteristics of the spatial distribution of cloud cover for Dome A and its surrounding areas in January, April, July, and October 2017

Month	μ/(%)	σ/(%)	CV	Range/(%)	Spatial distribution
January	30.50	2.48	0.08	10	The cloud cover is moderate, with almost no fluctuation.
April	7.38	1.41	0.19	4	The cloud cover is extremely low, with almost no fluctuation.
July	19.00	0.97	0.05	3	The cloud cover is low, with almost no fluctuation.
October	41.31	16.78	0.41	48	The cloud cover is relatively high, with significant fluctuation.

4. TOTAL PRECIPITATION AND ATMOSPHERIC WATER VAPOR

Precipitation in Antarctica typically falls to the ground in the form of rain, snow, or sleet, thereby carrying heat into the snowpack and altering the structure and albedo of the snow. Spatial distribution and variability of precipitation also influence the clear-sky rate, affecting the ability of telescopes to conduct continuous observations. In this study, we used the ERA5 dataset to conduct a statistical analysis of the total precipitation data for the specified region (76.96°E–77.96°E, 79.88°S–80.88°S) during January, April, July, and October 2017[12]. This analysis explored the seasonal variations and spatial distribution characteristics of precipitation and provided an assessment of the suitability of this region for astronomical observations.

Fig. 3 shows the annual average precipitation in millimeters for each grid cell (spatial unit corresponding to the latitude and longitude resolution of the original dataset) for Dome A and its surrounding area, taken as the average of 12 months. The values for each grid cell range from 0.52 to 0.83 mm. Fig. 4 shows the average precipitation, in millimeters, for each grid cell in January, April, July, and October, which was 0.07–0.18 mm, 0.05–0.06 mm, 0.04–0.07 mm, and 0.03–0.05 mm, respectively. Fig. 3 and Fig. 4 also show images generated from the original data that have undergone interpolation smoothing. This processing only improves the spatial smoothness of the images and does not affect the expression of the statistical trends in the original data. Its purpose is to more clearly show the spatial distribution characteristics.

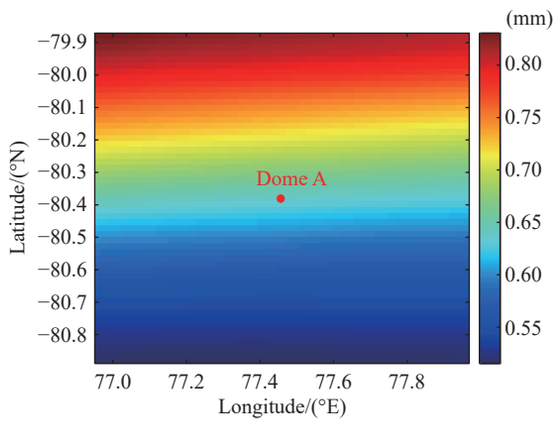

Fig. 3. Distribution of mean total precipitation at Dome A and its surroundings in 2017.

In terms of spatial distribution, within a 1° × 1° area centered on Dome A (77.45°E, 80.38°S), total precipitation shows a north-to-south gradient distribution along the latitude, except in October. Fig. 5 refers to the total precipitation for the entirety of Dome A and its surrounding areas over 12 months in 2017. It is the sum of the precipitation values for all grid cells in the study area and represents the cumulative total for the region, rather than the value for a single grid cell. The total precipitation for January, April, July, and October 2017 was 14.25 mm, 6.47 mm, 6.44 mm, and 4.78 mm, respectively. Precipitation remained at relatively low levels from March to December, including the polar night period (April to July), indicating that the site possesses stable and favorable atmospheric conditions. We found that the period from April to July is the optimal time for optical astronomical observations.

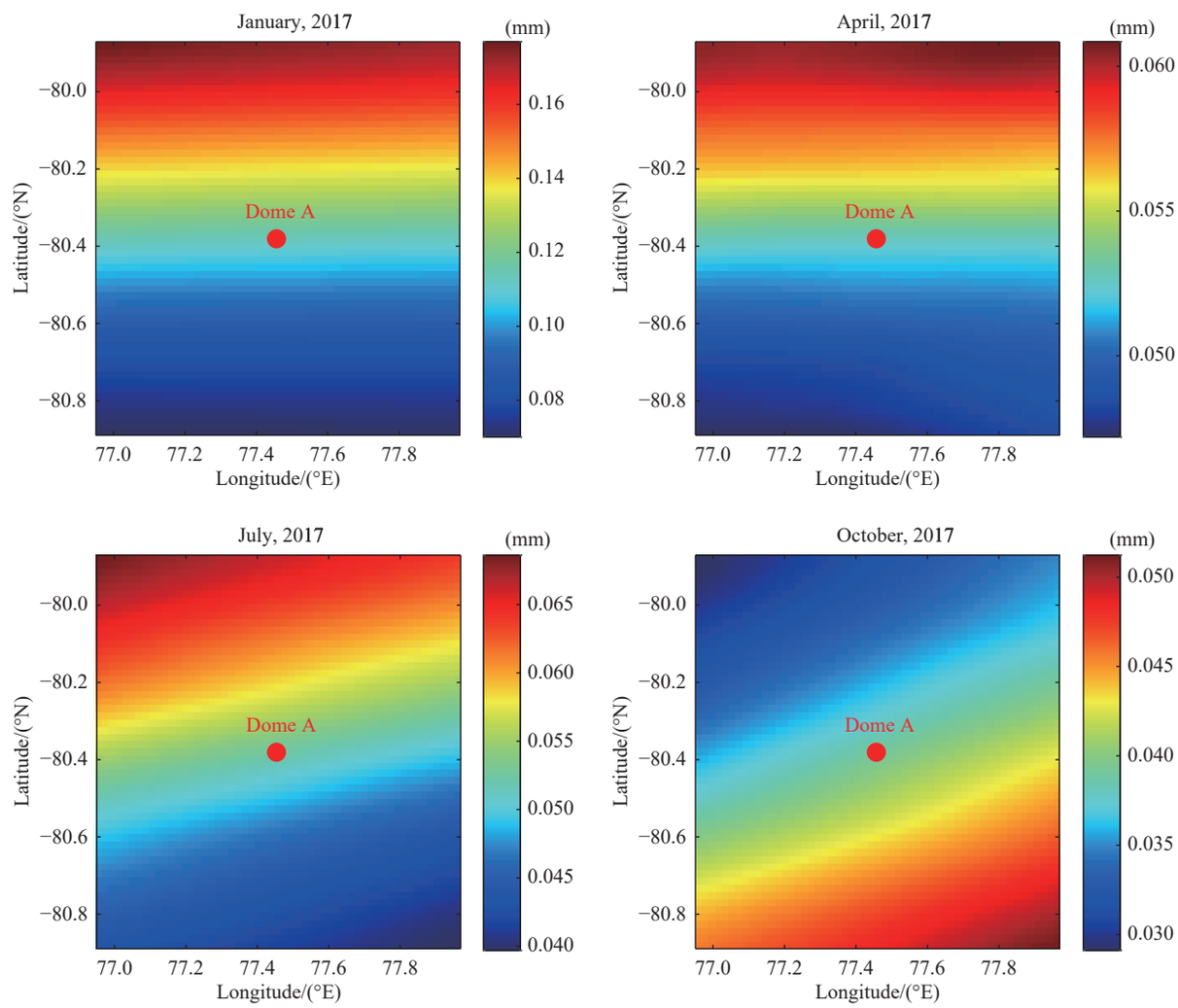

Fig. 4. Distribution of mean total precipitation at Dome A and its surroundings in January, April, July, and October 2017.

In addition to total precipitation, we analyzed the 2017 total column water vapor (TCWV) at Dome A and surrounding areas using the ERA5 reanalysis dataset from the Climate Data Store (CDS)[13]. Fig. 6 shows the mean TCWV at Dome A and its surrounding areas in 2017. Fig. 7 shows the mean TCWV for January, April, July, and October 2017 at Dome A and its surrounding areas, with mean TCWV ranges of 0.542–0.586 kg m^{-2}, 0.157–0.165 kg m^{-2}, 0.136–0.145 kg m^{-2}, and 0.207–0.215 kg m^{-2}. Fig. 8 illustrates the monthly mean TCWV trends for Dome A and its surrounding areas in 2017, with TCWV values of 0.559 kg m^{-2}, 0.159 kg m^{-2}, 0.138 kg m^{-2}, and

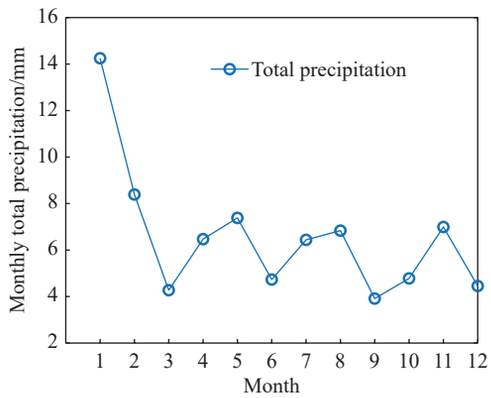

Fig. 5. Monthly changes in total precipitation at Dome A and the surrounding area in 2017.

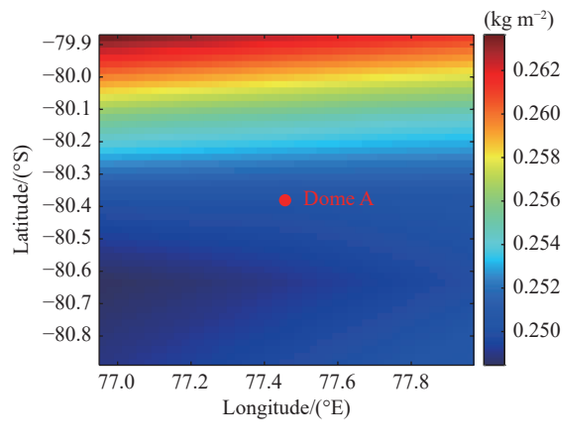

Fig. 6. Mean TCWV for Dome A and its surrounding region in 2017.

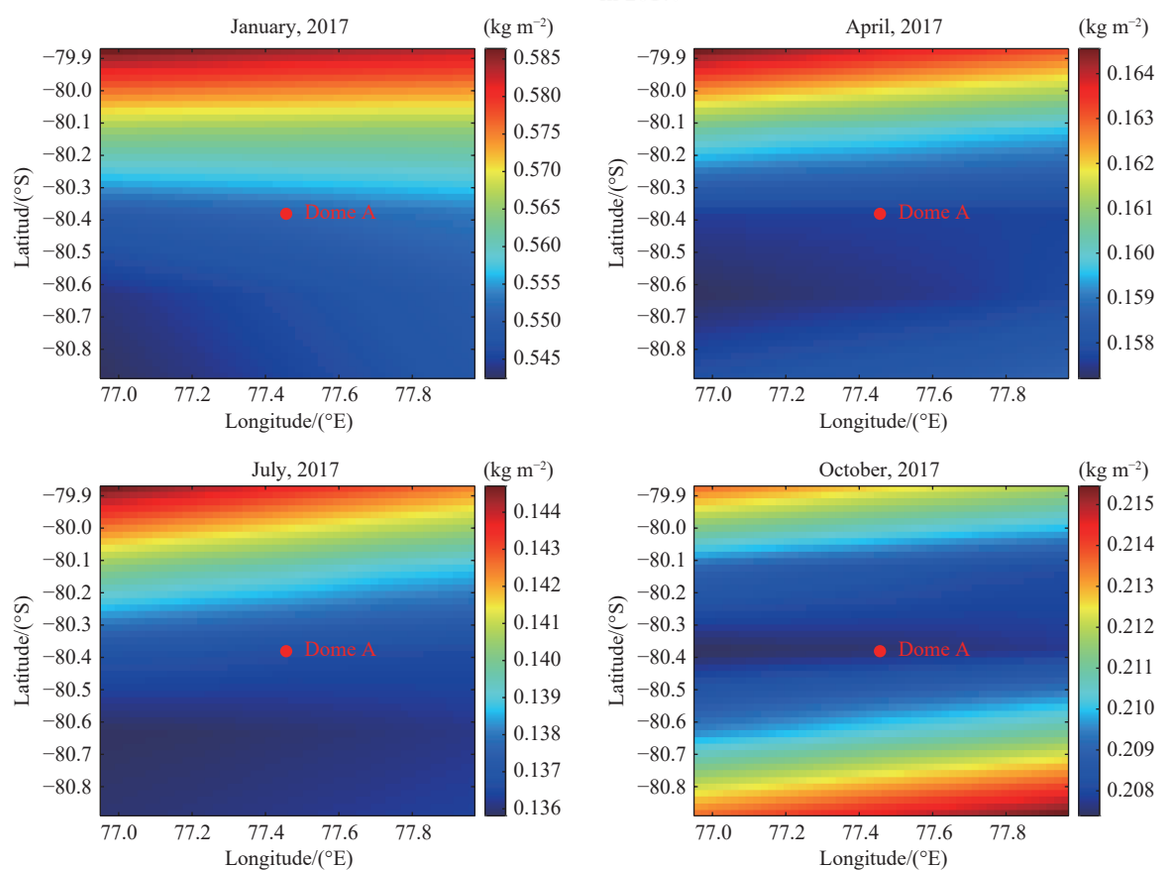

Fig. 7. Mean TCWV for Dome A and its surrounding region in January, April, July, and October 2017.

0.210 kg m^{-2} for January, April, July, and October 2017, respectively.

To further assess the observational conditions at Dome A and its surrounding areas, we compared them with those from other well-known astronomical observatory sites. According to Deng et al.[14], at the Lenghu site, 55% of the total nights throughout the year showed precipitable water vapor (PWV) below 2 mm, while at Mauna Kea, 54% of the total nights throughout the year had PWV below 2 mm. By contrast, the TCWV at Dome A and its surrounding areas was even lower, especially during polar night. The mean annual TCWV for Dome A and its surrounding areas in 2017 was 0.254 kg m^{-2} (equivalent to 0.254 mm). Notably, the statistical methods for TCWV used in this study differed from those for PWV used in previously published literature. However, this study's finding still reflects the extremely low atmospheric water vapor at Dome A. This is advantageous for infrared and submillimeter astronomical observations, further validating the suitability of this site for astronomy.

5. SKIN TEMPERATURE

In addition to precipitation factors, skin temperature

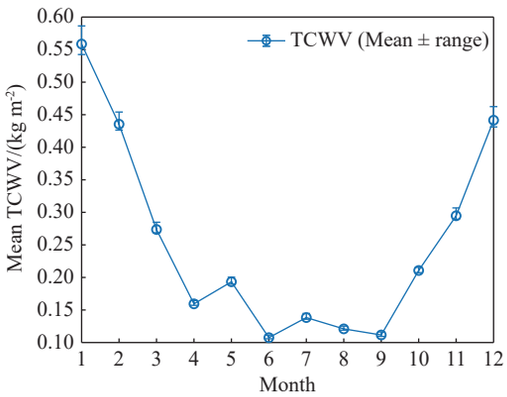

Fig. 8. Monthly mean TCWV for Dome A and its surrounding areas in 2017.

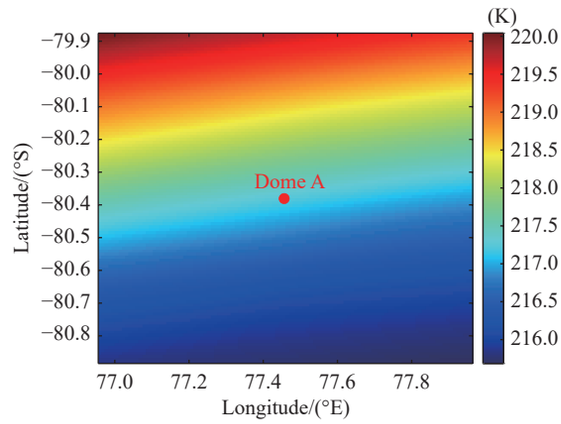

Fig. 9. Mean skin temperature for Dome A and its surrounding areas in 2017.

is a significant meteorological variable that influences astronomical observation conditions. To enhance the meteorological suitability assessment for astronomical observation site selection, we included the incorporation of skin temperature as an evaluation factor derived from cloud cover and precipitation analysis. We conducted a statistical analysis of the target region (76.96°E–77.96°E, 79.88°S–80.88°S) using data from the ERA5 dataset for four representative months in 2017[12]. Figs. 9 and 10 show the mean skin temperatures of Dome A and its surrounding areas in 2017, as well as the mean skin temperatures in January, April, July, and October 2017. The ranges of mean skin temperatures were 230.37–236.77 K, 208.26–214.01 K, 205.89–208.86 K, and 217.42–221.93 K, with corresponding mean skin temperatures for each month of 237.85 K, 210.72 K, 206.86 K, and 219.19 K, respectively. The skin temperature of Dome A and its surrounding areas was observed to be generally low, with April and July showing lower temperatures than those in the other two months. This finding suggests that atmospheric radiative cooling is significant during polar night. Fig. 11 shows a summary of the monthly mean skin temperature trends for Dome A and its surrounding areas in 2017. To verify the reliability of the ERA5 reanalysis data used in this study, the mean skin temperatures from ERA5 for January, February, and March 2017 were compared with the ground-level (0 m) temperature monitored by the temperature sensor equipped on the AST3-2 telescope at Dome A during the same period. The results show that the mean skin temperature derived from the ERA5 reanalysis data for these three months was 227.2 K (−45.95°C), while the observed ground-level temperature averaged −45.65°C. The close agreement between these values indicates that the ERA5 reanalysis data reliably represents surface temperature in this region.

In terms of spatial distribution, skin temperature showed a longitudinal gradient across the Dome A region, with the lowest temperature recorded in the southeastern region within the 1° × 1° area surrounding Dome A (centered on 77.45°E, 80.38°S). We evaluated the spatial variability within this area using a combination of the CV, σ, and μ. As shown in Table 2, the results of this analysis indicate that skin temperatures were at their lowest in April and July, with a smaller and more evenly distributed temperature difference in July. Accordingly, the eastern region is recommended as ideal for astronomical observations in July.

6. VWS

VWS is an important atmospheric parameter that influences the stability of the atmosphere and, consequently, the quality of astronomical observations. Although it is related to atmospheric seeing, this section focuses specifically on quantifying and analyzing VWS over Dome A.

VWS is primarily influenced by three factors. First, free-atmosphere turbulence arises from instabilities in the airflow of the upper atmosphere, causing scintillation of starlight, with VWS being the primary driving mechanism behind this turbulence. Another factor is boundary-layer turbulence, associated with near-surface wind speed. This includes both mechanical turbulence and thermal convection near the ground. Finally, the height of the boundary layer also plays an important role, with a lower boundary layer generally being more favorable because it helps to minimize the influence of ground-layer turbulence on astronomical observations.

To effectively analyze the VWS conditions over Dome A, we employed the ERA5 reanalysis dataset, released by the CDS platform[15], as the primary data source for evaluating the net surface solar radiation in the study area. We selected the U-component and V-component of wind data for January, April, July, and October 2017 over Dome A and its surrounding regions. The data have a temporal resolution of 1 h (accumulated values), and we chose pressure levels of 600 hPa, representing the lower troposphere, and 350 hPa, representing the upper troposphere, to construct vertical wind profiles. These profiles were then used to further analyze the structure of VWS.

We adopted the 600 hPa pressure level (approximately 4370 m above sea level) as a representative lower-atmospheric height for estimating near-surface wind

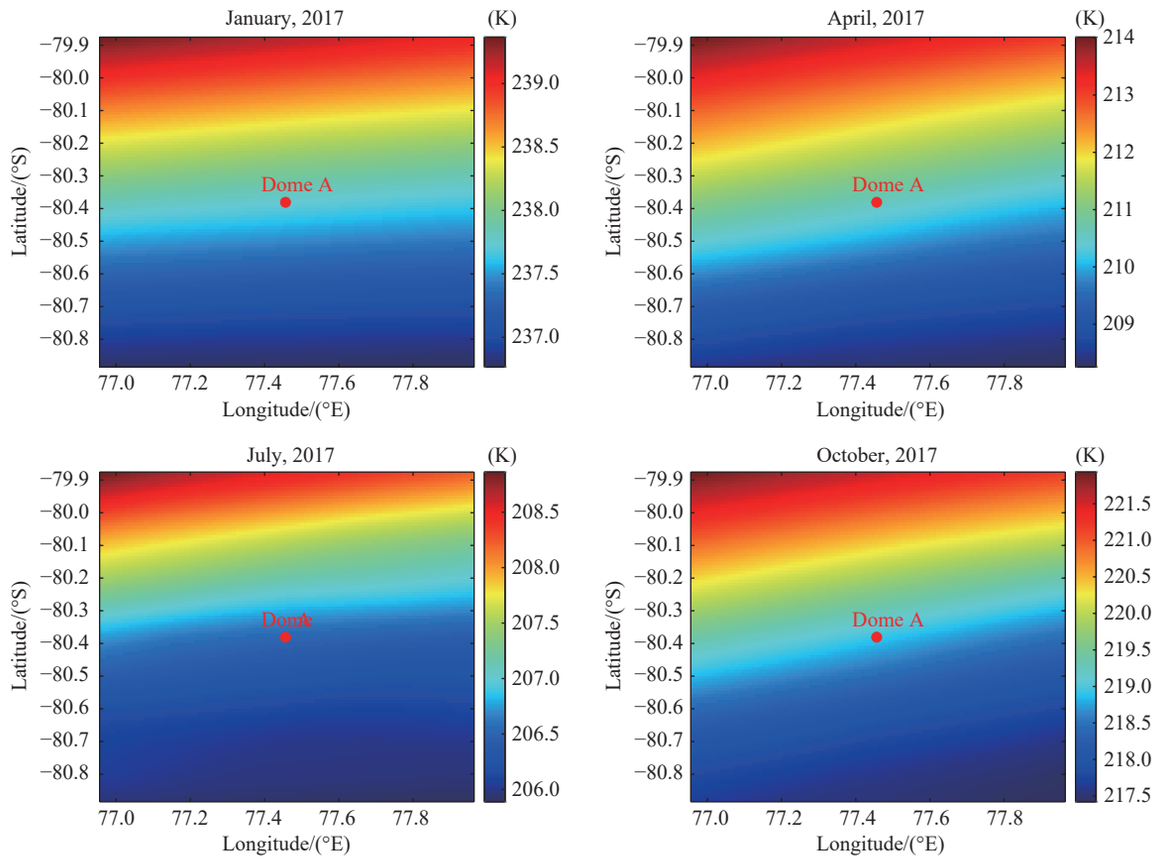

Fig. 10. Mean skin temperature for Dome A and its surrounding areas in January, April, July, and October 2017.

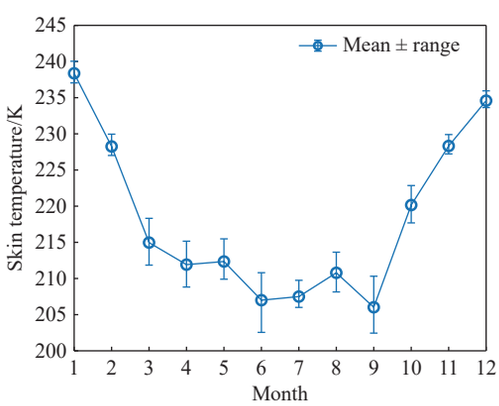

Fig. 11. Monthly mean skin temperature variations for Dome A and its surrounding areas in 2017.

speed. Owing to the vertical resolution of 50 hPa in the ERA5 dataset, we selected 600 hPa as the closest available pressure level to the surface elevation of Dome A. The scalar wind speed at 600 hPa (denoted as WS_{600}, in units of m s^{-1}) at each spatial grid point is calculated as

$$WS_{600} = \sqrt{U_{600}^2 + V_{600}^2}\,, \tag{1}$$

where U_{600} and V_{600} represent the zonal and meridional wind components at the 600 hPa level, respectively.

Similarly, the upper-level wind speed is represented by the wind speed at the 350 hPa pressure level (approximately 7370 m), which characterizes the upper tropospheric flow. Owing to the limitations of the standard pressure levels in the ERA5 dataset, higher vertical resolution data that accurately cover the boundary layer height (with a typical median of only 15 m) are not available. Consequently, within the accessible vertical levels, we selected the 350–600 hPa wind shear index as an indirect representation of the upper-atmosphere wind structure, aiming to explore potential variations in large-scale dynamic patterns rather than directly describing turbulence characteristics within the boundary layer. The scalar wind speed at

Table 2. Statistical characteristics of the spatial distribution of skin temperature for Dome A and its surrounding areas in January, April, July, and October 2017.

Month	μ/K	σ/K	CV	Range/K	Interquartile range (IQR)/K	Spatial distribution
January	237.85	0.79	0.0033	2.60	1.39	Higher and uniform skin temperatures
April	210.72	1.70	0.0081	5.75	2.99	Extremely low and uniform skin temperatures
July	206.86	0.87	0.0042	2.97	1.45	Extremely low and uniform skin temperatures
October	219.19	1.37	0.0062	4.51	2.46	Lower and uniform skin temperatures

350 hPa (denoted as WS_{350}, in units of m s^{-1}) at each spatial grid point is calculated as

$$WS_{350} = \sqrt{U_{350}^2 + V_{350}^2}\,, \tag{2}$$

where U_{350} and V_{350} denote the zonal and meridional wind components at the 350 hPa level, respectively.

VWS is an important metric used to quantify the variation in wind speed between different atmospheric layers, in units of m/s/km. It has a significant impact on atmospheric turbulence and astronomical seeing, and is given by

$$VWS = \frac{WS_{350} - WS_{600}}{\Delta h} \times 1\,000\,, \tag{3}$$

where Δh represents the difference in altitude, in units of m.

On the basis of ERA5 reanalysis data, our analysis indicates that VWS and near-surface wind speed in the target region show pronounced seasonal variation. As shown in Fig. 12, the mean near-surface wind speed over Dome A and its surrounding region during January, April, July, and October of 2017 falls in ranges of 3.89–4.96 m s^{-1}, 5.39–7.06 m s^{-1}, 5.39–5.99 m s^{-1}, and 5.28–8.16 m s^{-1}, respectively. As shown in Fig. 13, the mean VWS over Dome A and its surrounding region during January, April, July, and October of 2017 is in the ranges 1.73–2.06 m/s/km, 1.51–1.91 m/s/km, 1.93–2.13 m/s/km, and 1.41–2.39 m/s/km, respectively.

The spatial variability of both near-surface wind speed and vertical wind shear was further evaluated using statistical indicators. The results are summarized in Tables 3 and 4, respectively. As shown in Table 3, near-surface wind speeds were generally higher in October, with the strongest spatial fluctuations occurring in October, whereas July exhibited the most uniform distribution. Similarly, Table 4 indicates that vertical wind shear was relatively stable in July, suggesting that this period features a more homogeneous atmospheric structure and provides favorable conditions for astronomical observations.

Regarding spatial distribution, VWS in the northern part of the study area was generally low, while near-surface wind speed tended to be relatively high. Notably, near-surface wind speeds in April and October were comparatively higher. October showed the greatest variability, characterized by a standard deviation of 0.94 m s^{-1} and a CV of 0.14. By contrast, near-surface wind speed in July showed low variability and moderate mean values, with the most uniform spatial distribution, indicating a relatively stable atmospheric state. At the same time, VWS in July was also relatively stable, with a low coefficient of variation. These data suggest that July features a more homogeneous atmospheric structure and provides prefer-

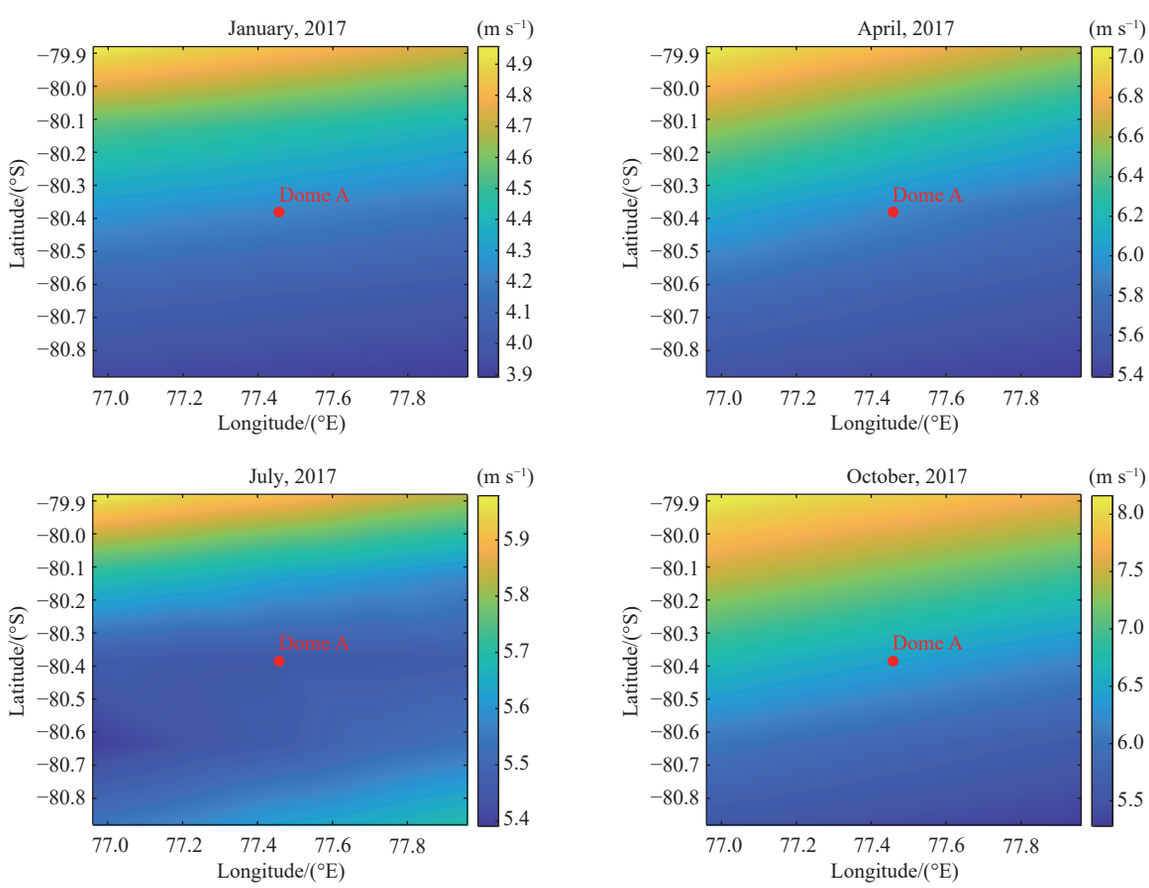

Fig. 12. Mean near-surface wind speed at 600 hPa over Dome A and its surrounding region in January, April, July, and October 2017.

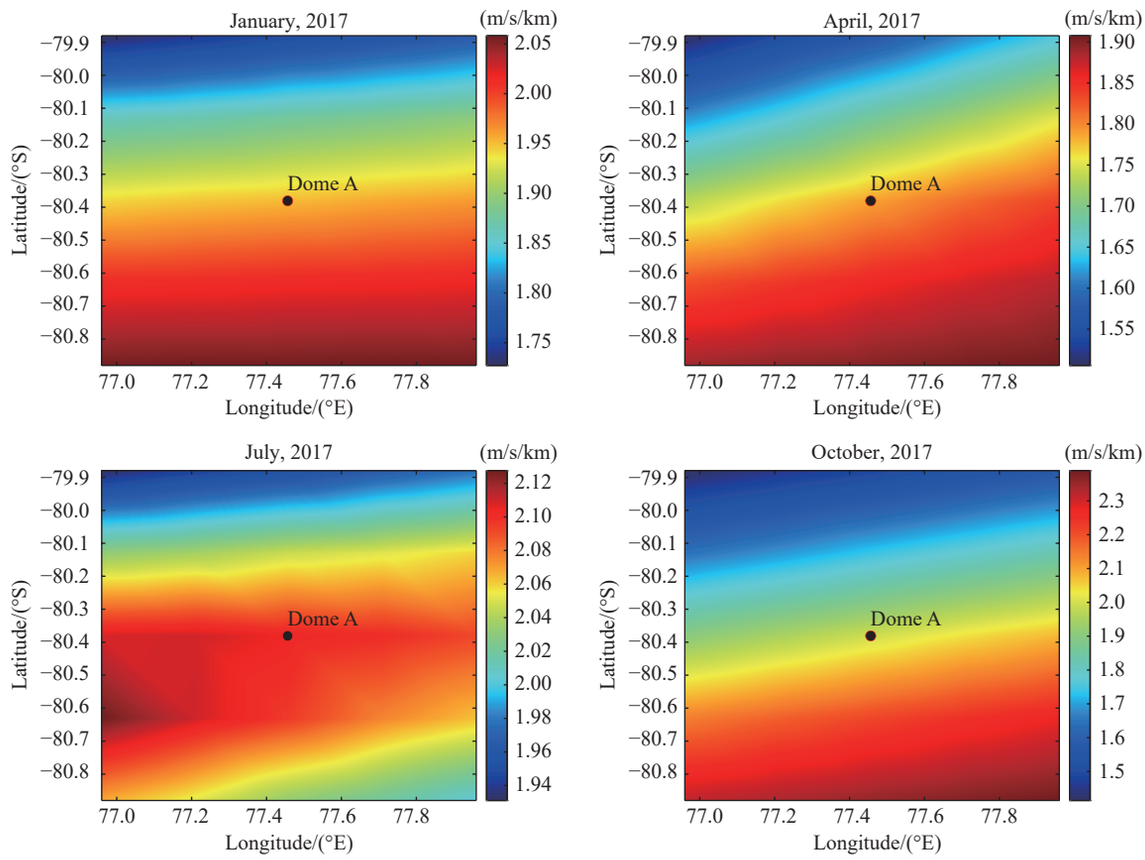

Fig. 13. VWS (350–600 hPa) over Dome A and its surrounding region in January, April, July, and October 2017.

Table 3. Statistical indicators of mean near-surface wind speed over Dome A and its surrounding region in January, April, July, and October 2017

Month	μ/(m s^{-1})	σ/(m s^{-1})	CV	Range/(m s^{-1})	IQR/(m s^{-1})	Spatial distribution
January	4.29	0.34	0.08	1.07	0.50	Relatively low overall wind speed
April	6.03	0.58	0.09	1.67	0.91	Wind speed strengthens overall, especially in the northwest
July	5.62	0.17	0.03	0.59	0.23	Uniform wind speed with minimal spatial variation
October	6.55	0.94	0.14	2.88	1.68	Large fluctuations, with higher wind speeds in the northwest

Table 4. Statistical indicators of mean VWS over Dome A and its surrounding region in January, April, July, and October 2017

Month	μ/ (m/s/km)	σ/ (m/s/km)	CV	Range/ (m/s/km)	IQR/ (m/s/km)	Spatial distribution
January	1.93	0.11	0.0566	0.33	0.15	Small wind speed fluctuations between the upper and lower levels
April	1.76	0.13	0.0710	0.40	0.22	Small wind speed fluctuations between the upper and lower levels
July	2.05	0.06	0.0279	0.20	0.08	Small wind speed fluctuations between the upper and lower levels
October	1.96	0.32	0.1657	0.97	0.57	Large wind speed fluctuations between the upper and lower levels

able conditions for astronomical observations.

7. SURFACE NET SOLAR RADIATION

To further assess the radiative characteristics of the astronomical observation environment, we utilized the ERA5 reanalysis dataset released by the CDS platform[13]. Surface net solar radiation data were selected for January, April, July, and October 2017, with a temporal resolution of one-hour accumulated values. Fig. 14 shows the analysis and calculation results of surface net solar radiation over the target region (76.96°E–77.96°E, 79.88°S–80.88°S) for January, April, July, and October of 2017, and Table 5 presents the data characteristics for different seasonal months. We used these data to systematically examine the seasonal variation patterns and spatial distribution characteristics of surface net solar radiation, to evaluate their potential impact on the suitability for astronomical observations.

The spatial variability of surface net solar radiation in the target region was comprehensively evaluated using σ, μ, and CV. In January, the CV was only 0.41, and the mean value reached 61.96 W m^{-2}, indicating that the region experiences relatively high solar radiation intensity with a uniform spatial distribution and low spatial vari-

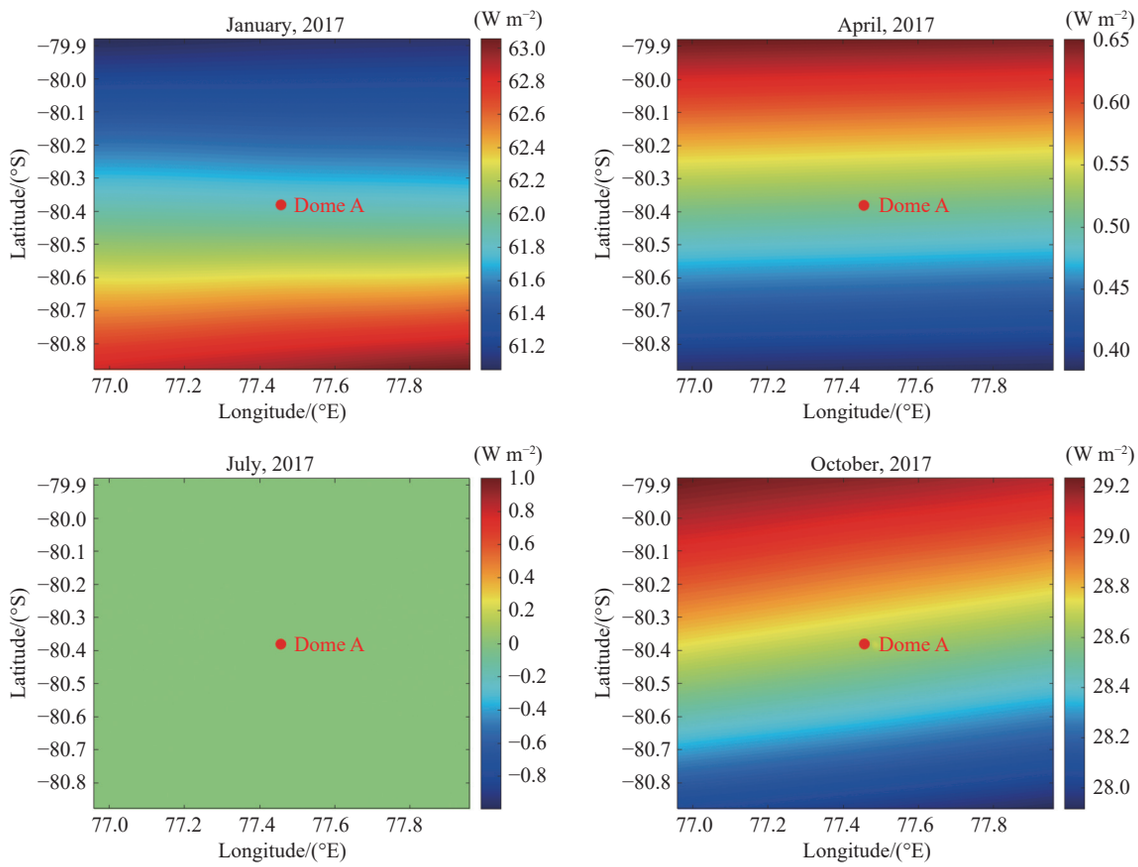

Fig. 14. Spatial distribution of net surface solar radiation over Dome A and its surrounding region in January, April, July, and October 2017.

Table 5. Statistical summary of net surface solar radiation over Dome A and its surrounding region in January, April, July, and October 2017

Month	μ/(W m^{-2})	σ/(W m^{-2})	CV	Spatial distribution
January	61.95	25.48	0.41	High values are uniformly distributed with low variability
April	0.52	1.93	3.78	Very low solar radiation across the entire region, with large variability
July	0	0	0	No solar radiation across the entire region
October	28.63	23.36	0.82	Low mean levels exhibiting moderate fluctuations

ability. In April, the solar elevation angle decreased significantly, resulting in a mean net surface solar radiation of only 0.52 W m^{-2}. Concurrently, the CV reached 3.78, indicating that although the overall solar radiation over Dome A and its surrounding region was very low, a degree of spatial variability existed. Nevertheless, the overall conditions remained suitable for conducting optical astronomical observations. In July, which corresponds to the polar night period in Antarctica, σ, μ, and CV of net surface solar radiation were all zero, indicating a complete absence of solar illumination and variability. This finding reflects the natural characteristics of the Antarctic polar night, making it a valuable period for astronomical regional observations. In October, the mean net surface solar radiation reached 28.63 W m^{-2}, indicating that solar radiation in Antarctica begins to increase during this period. However, the radiation level remained relatively low, with moderate variability, reflecting a low mean value and relatively stable distribution characteristics. Nevertheless, considering the increased and uneven cloud cover during this time, observing conditions become more complex, and opportunities for astronomical observation are relatively limited.

Our comprehensive analysis indicates that the seasonal variation of net surface solar radiation has a decisive impact on the astronomical observation conditions in the target region. January falls in the Antarctic summer period with high solar radiation, making it suitable primarily for specific solar physics studies. Surface net solar radiation reaches its minimum in April and July, resulting in the lowest background brightness and minimal thermal disturbances. Coupled with the low cloud cover levels during this period, these environmental characteristics indicate favorable conditions for optical astronomical observations in this timeframe.

8. CONCLUSION

In this study, we systematically assessed the suitability of Dome A and its surrounding region in Antarctica

for astronomical observations. Using multisource remote sensing data and high-precision meteorological reanalysis datasets, we focused on key observational parameters, including cloud cover, precipitation, atmospheric water vapor, skin temperature, vertical wind shear, and net surface solar radiation, during four representative months of 2017: January, April, July, and October. The results indicate that Dome A not only shows extremely low cloud cover and precipitation characteristics but also has highly stable climatic features in terms of skin temperature and wind field structure. Notably, April and July are characterized by low cloud cover, reduced net solar radiation, and favorable vertical wind shear conditions, making them exceptionally suitable periods for optical astronomical observations. Dome A and its surrounding region possess excellent conditions for astronomy, with climatic and environmental stability and spatial homogeneity, making it a key strategic node within both Antarctic and global astronomical research networks. This study provides important scientific foundations for the expanded use of Dome A and the development of future astronomical infrastructure, while also offering strong support for the rational allocation and optimization of global astronomical observation resources.

ACKNOWLEDGEMENTS

This work was supported by the Space Debris Research Project, China (KJSP2020010102) and the National Key R&D Program of China (2022YFC2807 300).

AI DISCLOSURE STATEMENT

ChatGPT (GPT-4, OpenAl) was employed for code error checking during the calculations in this paper and for language and grammar checking of the article. The authors carefully reviewed, edited, and revised the ChatGPT-generated texts to their own preferences, assuming ultimate responsibility for the content of the publication.

AUTHOR CONTRIBUTIONS

Peng Jiang and Xiaoyan Li supervised the project, contributed to the conceptualization, and oversaw the technical workflow. Kaiwen Zheng and Kun Ma were responsible for data analysis and processing. Haosi Song, Tiancong Zhang, Shiyi Wang, and Han Wang acquired and organized the relevant datasets. Kaiwen Zheng and Jiali Chen jointly drafted the manuscript and edited it for language. All authors read and approved the final manuscript.

DECLARATION OF INTERESTS

The authors declare no competing interests.

REFERENCES

[1] Lu, H. P., Yuan, X. Y., Zhang, K. Y. 2014. Infrared background radiation removing design and simulation of Antarctic survey telescope. *Acta Optica Sinica*, **34**(11): 1122002.

[2] Ma, B., Shang, Z. H., Hu, Y., et al. 2020. Night-time measurements of astronomical seeing at Dome A in Antarctica. *Nature*, **583**: 771−774.

[3] Zhang, J., Zhang, Y. H., Tang, Q. J., et al. 2023. Sky-brightness measurements in J, H, and Ks bands at DOME A with NISBM and early results. *Monthly Notices of the Royal Astronomical Society*, **521**(4): 5624−5635.

[4] Du, F. J., Li, Z. Y., Yuan, X. Y. 2016. Chinese Antarctic Astronomical Progression and Expeditions. *Progress in Astronomy*, **34**: 43−50. (in Chinese)

[5] Yuan, X. Y., Cui, X. Q., Liu, G. R , et al. 2008. Chinese Small Telescope Array (CSTAR) for Antarctic Dome A. In Proceedings of SPIE.

[6] Ma, B., Hu, Y., Shang, Z. H., et al. 2020. Automation of the AST3 optical sky survey from Dome A, Antarctica. *Monthly Notices of the Royal Astronomical Society*, **496**(3): 2768−2775.

[7] Li, Z. Y., Cong, J. N., Wu, Z. X., et al. 2024. System design for a wide field-of-view Near-Infrared Telescope for Dome A in Antarctica. *Publications of the Astronomical Society of the Pacific*, **136**(11): 115002.

[8] Copernicus Climate Change Service (C3S), Climate Data Store (CDS). 2022. Cloud properties global gridded monthly and daily data from 1982 to present derived from satellite observations. Copernicus Climate Change Service (C3S) Climate Data Store (CDS). [Accessed on 2025−06−27]

[9] Saunders, W., Lawrence, J. S., Storey, J. W. V., et al. 2009. Where is the best site on Earth? Domes A, B, C, and F, and Ridges A and B. *Publications of the Astronomical Society of the Pacific*, **121**(883): 976.

[10] Shikhovtsev, A. Y., Bolbasova, L. A., Kovadlo, P. G., et al. 2020. Atmospheric parameters at the 6-m Big Telescope Alt-azimuthal site. *Monthly Notices of the Royal Astronomical Society*, **493**(1): 723−729.

[11] Yang, X., Shang, Z. H., Hu, K. L., et al. 2021. Cloud cover and aurora contamination at Dome A in 2017 from KLCAM. *Monthly Notices of the Royal Astronomical Society*, **501**(3): 3614−3620.

[12] Muñoz Sabater, J. 2019. ERA5-Land monthly averaged data from 1950 to present. Copernicus Climate Change Service (C3S) Climate Data Store (CDS). [Accessed on 2025−06−27]

[13] Hersbach, H., Bell, B., Berrisford, P., et al. 2023. ERA5 hourly data on single levels from 1940 to present. Copernicus Climate Change Service (C3S) Climate Data Store (CDS). [Accessed on 2025−06−27]

[14] Deng, L. C., Yang, F., Chen, X. D., et al. 2021. Lenghu on the Tibetan Plateau as an astronomical observing site. *Nature*, **596**(7872): 353−356.

[15] Hersbach, H., Bell, B., Berrisford, P., et al. 2023. ERA5 hourly data on pressure levels from 1940 to present. Copernicus Climate Change Service (C3S) Climate Data Store (CDS). [Accessed on 2025−06−27]